arXiv:1512.04971v1 [math.NA] 15 Dec 2015

On the mesh nonsingularity of the moving mesh PDE method*

Weizhang Huang† Lennard Kamenski‡

Abstract

The moving mesh PDE (MMPDE) method for variational mesh generation and adaptation is studied theoretically at the discrete level, in particular the nonsingularity of the obtained meshes. Meshing functionals are discretized geometrically and the MMPDE is formulated as a modified gradient system of the corresponding discrete functionals for the location of mesh vertices. It is shown that if the meshing functional satisfies a coercivity condition, then the mesh of the semi-discrete MMPDE is nonsingular for all time if it is nonsingular initially. Moreover, the altitudes and volumes of its elements are bounded below by positive numbers depending only on the number of elements, the metric tensor, and the initial mesh. Furthermore, the value of the discrete meshing functional is convergent as time increases, which can be used as a stopping criterion in computation. Finally, the mesh trajectory has limiting meshes which are critical points of the discrete functional. The convergence of the mesh trajectory can be guaranteed when a stronger condition is placed on the meshing functional. Two meshing functionals based on alignment and equidistribution are known to satisfy the coercivity condition. The results also hold for fully discrete systems of the MMPDE provided that the time step is sufficiently small and a numerical scheme preserving the property of monotonically decreasing energy is used for the temporal discretization of the semi-discrete MMPDE. Numerical examples are presented.

AMS 2010 MSC. 65N50, 65K10

Key Words. Variational mesh generation, mesh adaptation, moving mesh PDE, mesh nonsingularity, limiting mesh

Abbreviated title. On the mesh nonsingularity for the MMPDE method

1 Introduction

The variational method for mesh generation and adaptation has received considerable attention in the scientific computing community; e.g., see [3, 18, 20, 25, 30] and references therein. It generates an adaptive mesh as the image of a given reference mesh under a coordinate

*W.H. was supported in part by the University of Kansas GRF Award # 2301056.

†The University of Kansas, Department of Mathematics, Lawrence, KS 66045, U.S.A. (whuang@ku.edu).

‡Weierstrass Institute for Applied Analysis and Stochastics, Berlin, Germany (kamenski@wias-berlin.de).

transformation determined by a meshing functional. Such a functional is typically designed to measure difficulties in the numerical approximation of the physical solution and involve a user-prescribed metric tensor (monitor function) to control mesh adaptation. This method has the advantage that it makes it easy to incorporate mesh requirements (e.g., smoothness, adaptivity, or alignment) in the formulation of the functional [2]. It serves as not only a standalone method for mesh generation and adaptation but also a smoothing device for automatic mesh generation (e.g., see [5, 13]). Moreover, the variational method is the base for a number of adaptive moving mesh methods [15, 17, 18, 24].

A number of variational methods have been developed so far. For example, Winslow [31] proposes an equipotential method based on variable diffusion. Brackbill and Saltzman [2] develop a method by combining mesh concentration, smoothness, and orthogonality. Dvinsky [4] uses the energy of harmonic mappings as his meshing functional. Knupp [21] and Knupp and Robidoux [22] formulate functionals based on the idea of conditioning the Jacobian matrix of the coordinate transformation. Huang [10] and Huang and Russell [18] develop functionals based on the so-called equidistribution and alignment conditions.

Compared with the algorithmic development, much less progress has been made in theoretical studies. The existence and uniqueness of the minimizer of Dvinsky's meshing functional is guaranteed by the theory of harmonic mappings between multidimensional domains [4]. Winslow's functional [31] is uniformly convex and coercive so it has a unique minimizer [18, Example 6.2.1]. Huang's functional [10] is coercive and polyconvex and has minimizers [18, Example 6.2.2] while that of Huang and Russell is coercive and polyconvex and has a nonsingular minimizer [18, Example 6.2.3]. Note that the nonsingularity of the minimizer for the above mentioned functionals is unknown (except for that of Huang and Russell). Moreover, these results are only at the continuous level.

At the discrete level, studies mainly remain in one spatial dimension. Pryce [27] proves the existence of the limiting mesh and the convergence of de Boor's algorithm for solving the equidistribution principle when the metric tensor is approximated by a piecewise linear interpolant. His result is generalized by Xu et al. [32] to the situation where the metric tensor is approximated by a piecewise constant interpolant. Gander and Haynes [6] and Haynes and Kwok [9] show the existence of the limiting mesh and the convergence of the parallel and alternating Schwarz domain decomposition algorithms applied to the continuous and discrete equidistribution principle.

The objective of this paper is to present a theoretical study on variational mesh generation and adaptation at the discrete level for any dimension. We consider a broad class of meshing functionals and the MMPDE method for finding their minimizers. We employ a geometric discretization recently introduced in [12] for meshing functionals. The semi-discrete MMPDE (discrete in space and continuous in time) is defined as a modified gradient system for the corresponding discrete functionals. The mesh nonsingularity and the existence and uniqueness of limiting meshes for both the semi-discrete and fully discrete MMPDEs are studied. Largely thanks to the inherent properties of the new discretization, it can be shown that if the meshing functional satisfies a coercivity condition, the mesh of the semi-discrete MMPDE stays nonsingular for all time if it is nonsingular initially. Moreover, the altitudes and volumes

of its elements are bounded from below by positive numbers depending only on the number of elements, the metric tensor, and the initial mesh. Furthermore, the value of the discrete functional is convergent as time increases, which can be used as a stopping criterion for the computation. Finally, the mesh trajectory has limiting meshes which are critical points of the discrete functional. The convergence of the mesh trajectory can be guaranteed when a stronger condition is placed on the meshing functional (see the discussion following Theorem 4.4). The functionals based on alignment and equidistribution [10, 18] are known to satisfy the coercivity condition for a large range of parameters (see (11) with $p > 1$). The analysis also holds for a fully discrete system for the MMPDE provided that the time step is sufficiently small and a numerical scheme preserving the property of monotonically decreasing energy is used to integrate the semi-discrete MMPDE. Euler, backward Euler, and algebraically stable Runge-Kutta schemes (including Gauss and Radau IIA) are known to preserve the property under a time-step restriction that involves a local Lipschitz bound of the Hessian matrix of the discrete functional (e.g., [8, 29]).

An outline of this paper is given as follows. Meshing functionals and the MMPDE method for finding minimizers are described in Sect. 2. The geometric discretization of the meshing functionals is given in Sect. 3. Section 4 is devoted to the analysis of the semi-discrete MMPDE and its discretization. Numerical examples are given in Sect. 5 to demonstrate the theoretical findings. The conclusions are drawn in Sect. 6.

2 Meshing functionals and MMPDE

In this section we describe the general form of a functional and two specific examples used for mesh generation and adaptation. We also discuss the concept of functional equivalence and the MMPDE approach for finding a minimizer of the meshing functional.

Let Ω be a bounded, not necessarily convex, polygonal or polyhedral domain in $\mathbb{R}^d$, $d \geq 1$, and $\mathbb{M} = \mathbb{M}(\boldsymbol{x})$ a symmetric metric tensor defined on Ω which satisfies

$$\underline{m}\, I \leq \mathbb{M}(\boldsymbol{x}) \leq \overline{m}\, I \quad \forall \boldsymbol{x} \in \Omega, \tag{1}$$

where the inequality sign is in the sense of positive definiteness and $\underline{m}, \overline{m} > 0$ are constants. Our goal is to use the variational method to generate a simplicial mesh for Ω according to $\mathbb{M}$.

Let Ω_c be a chosen computational domain, which can be a real domain in $\mathbb{R}^d$ or a collection of simplexes (see the discussion in the next section). With the variational method, an adaptive mesh is generated as the image of a computational mesh on Ω_c under a coordinate transformation between Ω_c and Ω which in turn is determined as a minimizer of a meshing functional.

Denote the coordinate transformation by $\boldsymbol{x} = \boldsymbol{x}(\boldsymbol{\xi}) : \Omega_c \to \Omega$ and its inverse coordinate transformation by $\boldsymbol{\xi} = \boldsymbol{\xi}(\boldsymbol{x}) : \Omega \to \Omega_c$. We consider meshing functionals in the form

$$I[\boldsymbol{\xi}] = \int_{\Omega} G\left(\mathbb{J}, \det(\mathbb{J}), \mathbb{M}, \boldsymbol{x}\right)\, d\boldsymbol{x}, \tag{2}$$

where $\mathbb{J} = \frac{\partial \boldsymbol{\xi}}{\partial \boldsymbol{x}}$ is the Jacobian matrix of $\boldsymbol{\xi} = \boldsymbol{\xi}(\boldsymbol{x})$ and G is a given function which is sufficiently smooth with respect to all of its arguments. This functional is minimized for the coordinate

transformation subject to suitable boundary correspondence between $\partial\Omega$ and $\partial\Omega_c$. The form (2) is very general and includes many existing meshing functionals as special examples (e.g., [18, 20, 25] and Examples 2.1 and 2.2 below).

The functional (2) is formulated in terms of the inverse coordinate transformation $\boldsymbol{\xi}(\boldsymbol{x})$. It can be transformed into a mathematically equivalent functional expressed in terms of the coordinate transformation $\boldsymbol{x}(\boldsymbol{\xi})$. To explain this, we consider a coordinate transformation $(\boldsymbol{x}, \boldsymbol{\xi}) \to (\boldsymbol{u}, \boldsymbol{v})$ defined by

$$\boldsymbol{x} = \Phi(\boldsymbol{u}, \boldsymbol{v}), \quad \boldsymbol{\xi} = \Psi(\boldsymbol{u}, \boldsymbol{v}), \qquad \det\left(\frac{\partial(\boldsymbol{x}, \boldsymbol{\xi})}{\partial(\boldsymbol{u}, \boldsymbol{v})}\right) \neq 0, \tag{3}$$

where $\boldsymbol{u}$ and $\boldsymbol{v}$ are the new independent and dependent variables, respectively. The curve given by the equation $\boldsymbol{\xi} = \boldsymbol{\xi}(\boldsymbol{x})$ in the $\boldsymbol{x}$-$\boldsymbol{\xi}$ space corresponds to the curve given by some equation $\boldsymbol{v} = \boldsymbol{v}(\boldsymbol{u})$ in the $\boldsymbol{u}$-$\boldsymbol{v}$ space. Making the change of variables (3), we can transform the functional (2) into a new functional involving $\boldsymbol{u}$ and $\boldsymbol{v}$. The invariance of the Euler-Lagrange equation in calculus of variations (e.g., Gelfand and Fomin [7]) states that if $\boldsymbol{\xi} = \boldsymbol{\xi}(\boldsymbol{x})$ satisfies the Euler-Lagrange equation of (2), then $\boldsymbol{v} = \boldsymbol{v}(\boldsymbol{u})$ satisfies the Euler-Lagrange equation of the new functional. Thus, the minimizers of (2) can be obtained through the minimizers of the new functional, and vice versa. In this sense, we say (2) and the new functional are mathematically equivalent.

Consider a special coordinate transformation

$$\boldsymbol{x} = \Phi(\boldsymbol{u}, \boldsymbol{v}) \equiv \boldsymbol{v}, \quad \boldsymbol{\xi} = \Psi(\boldsymbol{u}, \boldsymbol{v}) \equiv \boldsymbol{u}, \tag{4}$$

which represents an interchange of the roles of the independent and dependent variables. Since the Jacobian matrix of (4) is

$$\frac{\partial(\boldsymbol{x}, \boldsymbol{\xi})}{\partial(\boldsymbol{u}, \boldsymbol{v})} = \begin{bmatrix} 0 & I \\ I & 0 \end{bmatrix},$$

which is nonsingular, the invariance of the Euler-Lagrange equation implies that the functional (2) is mathematically equivalent to

$$I[\boldsymbol{x}] = \int_{\Omega_c} \frac{G\left(\mathbb{J}, \det(\mathbb{J}), \mathbb{M}, \boldsymbol{x}\right)}{\det(\mathbb{J})}\, d\boldsymbol{\xi}, \tag{5}$$

which is obtained by interchanging the roles of its independent and dependent variables in (2). Notice that the new functional is still denoted by I without causing confusion. Indeed, from the equivalence, we can consider (2) as a functional for $\boldsymbol{\xi} = \boldsymbol{\xi}(\boldsymbol{x})$ (*the $\boldsymbol{\xi}$-formulation*) or for $\boldsymbol{x} = \boldsymbol{x}(\boldsymbol{\xi})$ (through the interchanging the roles of the independent and dependent variations, i.e., (5) (*the $\boldsymbol{x}$-formulation*).

In this work, we use the $\boldsymbol{x}$-formulation. We employ the MMPDE method (a time-transient approach [14, 15]) to find a minimizer of the functional (5). The MMPDE is defined as a modified gradient flow of (5),

$$\frac{\partial \boldsymbol{x}}{\partial t} = -\frac{P}{\tau}\frac{\delta I}{\delta \boldsymbol{x}}, \quad t > 0, \tag{6}$$

where $\frac{\delta I}{\delta \boldsymbol{x}}$ is the functional derivative of I with respect to $\boldsymbol{x}$, $\tau > 0$ is a constant parameter used to adjust the time scale of the equation, and P is a positive scalar function used to make the

equation to have some invariance properties (a choice of P will be given later for Examples 2.1 and 2.2). A discretization of (6) gives a system for the nodal velocities for the physical mesh. The interested reader is referred to [18] for detailed discussion on the discretization of MMPDEs. In the next section, we consider a direct discretization method with which the functional (2) (instead of MMPDEs) is discretized directly and the nodal velocity system is then obtained as a modified gradient system of the discretized functional.

Example 2.1 (The generalized Winslow functional). The first example is a generalization of Winslow's variable diffusion functional [31],

$$I[\boldsymbol{\xi}] = \int_\Omega \operatorname{tr}(\mathbb{J}\mathbb{M}^{-1}\mathbb{J}^T)\, d\boldsymbol{x}, \tag{7}$$

where $\operatorname{tr}(\cdot)$ denotes the trace of a matrix and $\mathbb{M}^{-1}$ serves as the diffusion matrix. This functional has been used by many researchers; e.g., [1, 16, 17, 24]. It is coercive and convex (in terms of $\boldsymbol{\xi} = \boldsymbol{\xi}(\boldsymbol{x})$) and therefore has a unique minimizer [18, Example 6.2.1].

For the discretization to be discussed in the next section, we need the derivatives of G with respect to $\mathbb{J}$, $\det(\mathbb{J})$, $\mathbb{M}$, and $\boldsymbol{x}$. They are

$$\begin{cases} G = \operatorname{tr}(\mathbb{J}\mathbb{M}^{-1}\mathbb{J}^T), \\ \frac{\partial G}{\partial \mathbb{J}} = 2\mathbb{M}^{-1}\mathbb{J}^T, \\ \frac{\partial G}{\partial \det(\mathbb{J})} = 0, \\ \frac{\partial G}{\partial \mathbb{M}} = -\mathbb{M}^{-1}\mathbb{J}^T\mathbb{J}\mathbb{M}^{-1}, \\ \frac{\partial G}{\partial \boldsymbol{x}} = 0. \end{cases} \tag{8}$$

Note that $\frac{\partial G}{\partial \mathbb{J}}$ and $\frac{\partial G}{\partial \mathbb{M}}$ are d-by-d matrices and $\frac{\partial G}{\partial \boldsymbol{x}}$ is a row vector of d components. They are expressed in the notation of scalar-by-matrix differentiation. For example, $\frac{\partial G}{\partial \mathbb{J}}$ is a d-by-d matrix defined as

$$\left(\frac{\partial G}{\partial \mathbb{J}}\right)_{ij} = \frac{\partial G}{\partial \mathbb{J}_{ji}}. \tag{9}$$

The chain rule for scalar-by-matrix differentiation reads as[1]

$$\frac{\partial G}{\partial t} = \operatorname{tr}\left(\frac{\partial G}{\partial \mathbb{J}}\frac{\partial \mathbb{J}}{\partial t}\right). \tag{10}$$

Using the definition of G and viewing $\mathbb{J}$ as a function of t, we have

$$\frac{\partial G}{\partial t} = \operatorname{tr}\left(\frac{\partial \mathbb{J}\mathbb{M}^{-1}\mathbb{J}^T}{\partial t}\right) = \operatorname{tr}\left(\frac{\partial \mathbb{J}}{\partial t}\mathbb{M}^{-1}\mathbb{J}^T + \mathbb{J}\mathbb{M}^{-1}\frac{\partial \mathbb{J}^T}{\partial t}\right) = \operatorname{tr}\left(2\mathbb{M}^{-1}\mathbb{J}^T\frac{\partial \mathbb{J}}{\partial t}\right).$$

By comparing this with the chain rule, we get

$$\frac{\partial G}{\partial \mathbb{J}} = 2\mathbb{M}^{-1}\mathbb{J}^T.$$

The other derivatives are obtained similarly.

[1]The interested reader is referred to [12] for more detailed discussion on scalar-by-matrix differentiation.

Regarding the choice of P, it is useful to make the MMPDE invariant under the scaling transformation $\mathbb{M} \to c \cdot \mathbb{M}$ for a positive number c since the mesh concentration is controlled by the distribution of $\mathbb{M}$ instead of its absolute value. A choice of P for this purpose for the current functional is

$$P = \det(\mathbb{M})^{\frac{1}{d}}.$$

□

Example 2.2 (Huang's functional). The second functional is

$$I[\boldsymbol{\xi}] = \theta \int_\Omega \sqrt{\det(\mathbb{M})}\Big(\mathrm{tr}(\mathbb{J}\mathbb{M}^{-1}\mathbb{J}^T)\Big)^{\frac{dp}{2}}\, d\boldsymbol{x} + (1-2\theta)d^{\frac{dp}{2}} \int_\Omega \sqrt{\det(\mathbb{M})}\left(\frac{\det(\mathbb{J})}{\sqrt{\det(\mathbb{M})}}\right)^p d\boldsymbol{x}, \quad (11)$$

where $0 \le \theta \le 1$ and $p > 0$ are dimensionless parameters. This functional was proposed by Huang [10] based on the so-called alignment and equidistribution conditions. Alignment and equidistribution are balanced by θ, with full alignment for $\theta = 1$ and full equidistribution for $\theta = 0$. For $0 < \theta \le \frac{1}{2}$, $dp \ge 2$, and $p \ge 1$, the functional is coercive and polyconvex (in terms of $\boldsymbol{\xi} = \boldsymbol{\xi}(\boldsymbol{x})$) and has a minimizer [18, Example 6.2.2]. Moreover, for $\theta = \frac{1}{2}$ it reduces to

$$I[\boldsymbol{\xi}] = \frac{1}{2}\int_\Omega \sqrt{\det(\mathbb{M})}\,\Big(\mathrm{tr}(\mathbb{J}\mathbb{M}^{-1}\mathbb{J}^T)\Big)^{\frac{dp}{2}}\, d\boldsymbol{x}, \quad (12)$$

which is coercive and convex (in terms of $\boldsymbol{\xi} = \boldsymbol{\xi}(\boldsymbol{x})$) and has a unique minimizer. Particularly, (12) gives the energy functional for a harmonic mapping from Ω to Ω_c when $dp/2 = 1$ (cf. [4]). Moreover, (12) and Winslow's functional (7) coinside when $dp/2 = 1$ and $\mathbb{M} = I$.

The derivatives of G are

$$\begin{cases} G = \theta\sqrt{\det(\mathbb{M})}\Big(\mathrm{tr}(\mathbb{J}\mathbb{M}^{-1}\mathbb{J}^T)\Big)^{\frac{dp}{2}} + (1-2\theta)d^{\frac{dp}{2}}\sqrt{\det(\mathbb{M})}\left(\frac{\det(\mathbb{J})}{\sqrt{\det(\mathbb{M})}}\right)^p, \\ \frac{\partial G}{\partial \mathbb{J}} = dp\theta\sqrt{\det(\mathbb{M})}\Big(\mathrm{tr}(\mathbb{J}\mathbb{M}^{-1}\mathbb{J}^T)\Big)^{\frac{dp}{2}-1}\mathbb{M}^{-1}\mathbb{J}^T, \\ \frac{\partial G}{\partial r} = p(1-2\theta)d^{\frac{dp}{2}}\det(\mathbb{M})^{\frac{1-p}{2}}\det(\mathbb{J})^{p-1}, \\ \frac{\partial G}{\partial \mathbb{M}} = -\frac{\theta dp}{2}\sqrt{\det(\mathbb{M})}\Big(\mathrm{tr}(\mathbb{J}\mathbb{M}^{-1}\mathbb{J}^T)\Big)^{\frac{dp}{2}-1}\mathbb{M}^{-1}\mathbb{J}^T\mathbb{J}\mathbb{M}^{-1} + \frac{\theta}{2}\sqrt{\det(\mathbb{M})}\Big(\mathrm{tr}(\mathbb{J}\mathbb{M}^{-1}\mathbb{J}^T)\Big)^{\frac{dp}{2}}\mathbb{M}^{-1} \\ \qquad + \frac{(1-2\theta)(1-p)d^{\frac{dp}{2}}}{2}\sqrt{\det(\mathbb{M})}\left(\frac{\det(\mathbb{J})}{\sqrt{\det(\mathbb{M})}}\right)^p\mathbb{M}^{-1}, \\ \frac{\partial G}{\partial \boldsymbol{x}} = 0. \end{cases} \quad (13)$$

A choice of P to make the MMPDE invariant under the scaling transformations of $\mathbb{M}$ for the current functional is

$$P = \det(\mathbb{M})^{\frac{p-1}{2}}.$$

□

3 A geometric discretization of meshing functionals

Let $\mathcal{T}_h = \{K\}$ be the target simplicial mesh on Ω and N and N_v the numbers of its elements and vertices, respectively. We assume that the computational mesh $\mathcal{T}_c = \{K_c\}$ is chosen such that

(a) it has the same N and N_v as $\mathcal{T}_h$,

(b) there is a one-to-one correspondence between the elements of $\mathcal{T}_c$ and those of $\mathcal{T}_h$,

(c) $\mathcal{T}_c$ has the same connectivity when $\mathcal{T}_c$ is a real mesh (see the explanation below),

(d) $\mathcal{T}_c$ is almost uniform (all of its elements have almost the same size and are almost equilateral).

$\mathcal{T}_c$ can be a real mesh or a collection of N simplexes. An example of the latter case is a $\mathcal{T}_c$ consisting of N copies of $(N^{-\frac{1}{d}}\hat{K})$, where $(N^{-\frac{1}{d}}\hat{K})$ denotes a unitary equilateral simplex $\hat{K}$ scaled by $N^{-\frac{1}{d}}$.

For any element $K \in \mathcal{T}_h$ and the corresponding element $K_c \in \mathcal{T}_c$, let $F_K : K_c \to K$ be the affine mapping between them and F_K' its Jacobian matrix. Let the vertices of K and K_c be $\boldsymbol{x}_j^K$, $j = 0, \ldots, d$ and $\boldsymbol{\xi}_j^K$, $j = 0, \ldots, d$, respectively. It holds

$$F_K' = E_K \hat{E}_K^{-1}, \quad (F_K')^{-1} = \hat{E}_K E_K^{-1}, \quad |K| = \frac{1}{d!}|\det(E_K)|, \quad |K_c| = \frac{1}{d!}|\det(\hat{E}_K)|, \tag{14}$$

where the edge matrices E_K and $\hat{E}_K$ are defined as

$$E_K = [\boldsymbol{x}_1^K - \boldsymbol{x}_0^K, \ldots, \boldsymbol{x}_d^K - \boldsymbol{x}_0^K], \quad \hat{E}_K = [\boldsymbol{\xi}_1^K - \boldsymbol{\xi}_0^K, \ldots, \boldsymbol{\xi}_d^K - \boldsymbol{\xi}_0^K].$$

Let

$$\Omega_c = \bigcup_{K_c \in \mathcal{T}_c} K_c.$$

Note that Ω_c may be a real domain in $\mathbb{R}^d$ or a collection of N simplexes.

We now describe the geometric discretization [12] for the functional (2). The idea is simple: the coordinate transformation $\boldsymbol{x} = \boldsymbol{x}(\boldsymbol{\xi})$ is approximated by the piecewise linear mapping $\{F_K,\ K \in \mathcal{T}_h\}$ and the integral in (2) is approximated by the midpoint quadrature rule.[2] This results in a Riemann sum which can be considered as a function of the location of the physical vertices (in the $\boldsymbol{x}$-formulation), according to the functional equivalence discussed in the preceding section. (Note that $\mathcal{T}_c$ is given and, thus, known.) From $\mathbb{J} \approx (F_K')^{-1} = \hat{E}_K E_K^{-1}$ on K, we have

$$I_h(\boldsymbol{x}_1, \ldots, \boldsymbol{x}_{N_v}) = \sum_{K \in \mathcal{T}_h} |K|\, G(\hat{E}_K E_K^{-1}, \frac{\det(\hat{E}_K)}{\det(E_K)}, \mathbb{M}_K, \boldsymbol{x}_K), \tag{15}$$

where $\boldsymbol{x}_K$ is the centroid of K and $\mathbb{M}_K = \frac{1}{d+1}\sum_{i=0}^{d} \mathbb{M}(\boldsymbol{x}_i^K)$. As for the continuous case, the MMPDE for (15) is defined as

$$\frac{d\boldsymbol{x}_i}{dt} = -\frac{P(\boldsymbol{x}_i)}{\tau}\left(\frac{\partial I_h}{\partial \boldsymbol{x}_i}\right)^T, \quad i = 1, \ldots, N_v,\ t > 0. \tag{16}$$

[2] A more accurate quadrature rule could be used; however, our numerical experience shows that the simple midpoint quadrature rule works well for problems tested.

The derivatives on the right-hand side of the mesh equation (16) can be found analytically in a compact matrix form (see [12] for the derivation):

$$\frac{d\boldsymbol{x}_i}{dt} = \frac{P(\boldsymbol{x}_i)}{\tau} \sum_{K\in\omega_i} |K| \boldsymbol{v}_{i_K}^K, \quad i = 1, \ldots, N_v, \tag{17}$$

where ω_i is the patch of the elements having $\boldsymbol{x}_i$ as one of their vertices and i_K and $\boldsymbol{v}_{i_K}^K$ are the local index and velocity of vertex $\boldsymbol{x}_i$ on the element K, respectively. The local velocities are

$$\begin{aligned}\begin{bmatrix} (\boldsymbol{v}_1^K)^T \\ \vdots \\ (\boldsymbol{v}_d^K)^T \end{bmatrix} =& - GE_K^{-1} + E_K^{-1} \frac{\partial G}{\partial \mathbb{J}} \hat{E}_K E_K^{-1} + \frac{\partial G}{\partial \det(\mathbb{J})} \frac{\det(\hat{E}_K)}{\det(E_K)} E_K^{-1} \\ & - \frac{1}{d+1} \sum_{j=0}^{d} \operatorname{tr}\left(\frac{\partial G}{\partial \mathbb{M}} \mathbb{M}_{j,K} \right) \begin{bmatrix} \frac{\partial \phi_{j,K}}{\partial \boldsymbol{x}} \\ \vdots \\ \frac{\partial \phi_{j,K}}{\partial \boldsymbol{x}} \end{bmatrix} - \frac{1}{d+1} \begin{bmatrix} \frac{\partial G}{\partial \boldsymbol{x}} \\ \vdots \\ \frac{\partial G}{\partial \boldsymbol{x}} \end{bmatrix}, \end{aligned} \tag{18}$$

$$(\boldsymbol{v}_0^K)^T = - \sum_{k=1}^{d} (\boldsymbol{v}_k^K)^T - \sum_{j=0}^{d} \operatorname{tr}\left(\frac{\partial G}{\partial \mathbb{M}} \mathbb{M}_{j,K} \right) \frac{\partial \phi_{j,K}}{\partial \boldsymbol{x}} - \frac{\partial G}{\partial \boldsymbol{x}}, \tag{19}$$

where $\mathbb{M}_{j,K} = \mathbb{M}(\boldsymbol{x}_j^K)$, $\phi_{j,K}$ is the linear basis function associated with $\boldsymbol{x}_j^K$, and

$$G, \quad \frac{\partial G}{\partial \mathbb{J}}, \quad \frac{\partial G}{\partial \det(\mathbb{J})}, \quad \frac{\partial G}{\partial \mathbb{M}}, \quad \text{and} \quad \frac{\partial G}{\partial \boldsymbol{x}}$$

are evaluated at

$$\mathbb{J} = \hat{E}_K E_K^{-1}, \quad \det(\mathbb{J}) = \frac{\det(\hat{E}_K)}{\det(E_K)}, \quad \boldsymbol{x} = \boldsymbol{x}_K.$$

The MMPDE (16) should be modified properly for boundary vertices: if $\boldsymbol{x}_i$ is a fixed boundary vertex, the corresponding equation is replaced by

$$\frac{d\boldsymbol{x}_i}{dt} = 0,$$

and when $\boldsymbol{x}_i$ is allowed to move on a boundary curve (in 2D) or surface (in 3D) represented by $\phi(\boldsymbol{x}) = 0$, then the mesh velocity $\frac{\partial \boldsymbol{x}_i}{\partial t}$ needs to be modified such that its normal component along the curve or surface is zero, i.e.,

$$\nabla \phi(\boldsymbol{x}_i) \cdot \frac{d\boldsymbol{x}_i}{dt} = 0.$$

Remark 3.1. The formulation of the MMPDE (16) is similar to that of a spring model for mesh movement (cf. [18, Section 7.3.2]), with the right-hand side term acting as the sum of the spring forces between $\boldsymbol{x}_i$ and its neighboring vertices. This makes it amenable to time integration by both explicit and implicit schemes. On the other hand, (16) is different from existing spring models for mesh movement. It does not involve parameters such as spring constants that typically need fine tuning. Moreover, the forces in (16) are defined based on the global meshing functional (2). This property is very important since it provides a good chance to prevent the mesh from becoming singular. For example, for the functional (11) the forces are defined to keep the mesh elements as regular and uniform in the metric $\mathbb{M}$ as possible. □

4 Mesh nonsingularity and existence of the limiting meshes

In this section we study the nonsingularity of the mesh trajectory and the existence of the limiting meshes as $t \to \infty$ for the semi-discrete MMPDE (16) and its discretization.

4.1 Two lemmas

The functionals in both Examples 2.1 and 2.2 involve a factor $\mathrm{tr}(\mathbb{J}\mathbb{M}^{-1}\mathbb{J}^T) = \mathrm{tr}((F_K')^{-1}\mathbb{M}_K^{-1}(F_K')^{-T})$. An equivalent form of it is $\|(F_K')^{-1}\mathbb{M}_K^{-1}(F_K')^{-T}\|$. We first obtain a geometric interpretation for it, which is needed later in our analysis.

Lemma 4.1. *Let $\hat{K}$ be an equilateral simplex and K an arbitrary simplex in $\mathbb{R}^d$, $F_K : \hat{K} \to K$ the affine mapping between them, and $\mathbb{M}_K$ a constant symmetric and positive definite matrix. Then,*

$$\frac{\hat{a}^2}{a_{K,\mathbb{M}}^2} \le \|(F_K')^{-1}\mathbb{M}_K^{-1}(F_K')^{-T}\| \le \frac{d^2\,\hat{a}^2}{a_{K,\mathbb{M}}^2}, \tag{20}$$

where $a_{K,\mathbb{M}}$ is the minimum altitude of K in the metric $\mathbb{M}_K$ and $\hat{a}$ is the altitude of $\hat{K}$.

Proof. Let $\hat{\phi}_i$ $(i = 0, \ldots, d)$ be the linear basis functions associated with the vertices of $\hat{K}$. It holds (e.g., Křížek and Lin [23] or Lu et al. [26, Lemma 1])

$$(\hat{\nabla}\hat{\phi}_i)^T\hat{\nabla}\hat{\phi}_i = \frac{1}{\hat{a}^2}, \quad i = 0, \ldots, d,$$

where $\hat{\nabla}$ is the gradient operator on $\hat{K}$ with respect to $\boldsymbol{\xi}$. (Recall that $\hat{K}$ is equilateral so all of its altitudes are the same.)

Let $\phi_i(\boldsymbol{x}) = \hat{\phi}_i(F_K^{-1}(\boldsymbol{x}))$, where F_K^{-1} is the inverse mapping of F_K. Since F_K is affine, ϕ_i is also a linear basis function on K. The altitudes of K in the metric $\mathbb{M}_K$ are related to the gradient of the linear basis functions by (cf. [26, (25) with $\mathbb{D}_K$ being replaced by $\mathbb{M}_K^{-1}$])

$$(\nabla\phi_i)^T\mathbb{M}_K^{-1}\nabla\phi_i = \frac{1}{a_{i,K,\mathbb{M}}^2},$$

where ∇ stands for the gradient operator on K with respect to $\boldsymbol{x}$. $\phi_i(\boldsymbol{x}) = \hat{\phi}_i(F_K^{-1}(\boldsymbol{x}))$ and the chain rule give

$$\nabla\phi_i = (F_K')^{-T}\hat{\nabla}\hat{\phi}_i.$$

We are now ready to prove (20):

$$\begin{aligned}
\|(F_K')^{-1}\mathbb{M}_K^{-1}(F_K')^{-T}\| &= \max_{\boldsymbol{v}\neq 0} \frac{\boldsymbol{v}^T(F_K')^{-1}\mathbb{M}_K^{-1}(F_K')^{-T}\boldsymbol{v}}{\boldsymbol{v}^T\boldsymbol{v}} \\
&\ge \frac{(\hat{\nabla}\hat{\phi}_i)^T(F_K')^{-1}\mathbb{M}_K^{-1}(F_K')^{-T}\hat{\nabla}\hat{\phi}_i}{(\hat{\nabla}\hat{\phi}_i)^T\hat{\nabla}\hat{\phi}_i} \\
&= \frac{(\nabla\phi_i)^T\mathbb{M}_K^{-1}\nabla\phi_i}{\hat{a}^{-2}} = \frac{\hat{a}^2}{a_{i,K,\mathbb{M}}^2},
\end{aligned}$$

which implies

$$\|(F_K')^{-1}\mathbb{M}_K^{-1}(F_K')^{-T}\| \geq \max_i \frac{\hat{a}^2}{a_{i,K,\mathbb{M}}^2} = \frac{\hat{a}^2}{a_{K,\mathbb{M}}^2}.$$

Thus, we obtained the left inequality of (20).

On the other hand, $\hat{\nabla}\hat{\phi}_i$, $i = 1, \ldots, d$, form a set of d linearly independent vectors. Thus, we can represent any $\boldsymbol{v} \in \mathbb{R}^d$ as

$$\boldsymbol{v} = \sum_{i=1}^{d} \alpha_i \hat{\nabla}\hat{\phi}_i.$$

Then,

$$\boldsymbol{v}^T\boldsymbol{v} = \sum_{i,j=1}^{d} \alpha_i\alpha_j \hat{\nabla}\hat{\phi}_i^T\hat{\nabla}\hat{\phi}_j$$

and

$$\begin{aligned}
\boldsymbol{v}^T(F_K')^{-1}\mathbb{M}_K^{-1}(F_K')^{-T}\boldsymbol{v} &= \sum_{i,j=1}^{d} \alpha_i\alpha_j \hat{\nabla}\hat{\phi}_i^T(F_K')^{-1}\mathbb{M}_K^{-1}(F_K')^{-T}\hat{\nabla}\hat{\phi}_j \\
&= \sum_{i,j=1}^{d} \alpha_i\alpha_j \nabla\phi_i^T\mathbb{M}_K^{-1}\nabla\phi_j \\
&= \sum_{i,j=1}^{d} \alpha_i\alpha_j (\mathbb{M}_K^{-\frac{1}{2}}\nabla\phi_i)^T(\mathbb{M}_K^{-\frac{1}{2}}\nabla\phi_j).
\end{aligned}$$

Thus,

$$\begin{aligned}
\boldsymbol{v}^T(F_K')^{-1}\mathbb{M}_K^{-1}(F_K')^{-T}\boldsymbol{v} &\leq \sum_{i,j=1}^{d} |\alpha_i|\,|\alpha_j| \frac{1}{a_{i,K,\mathbb{M}}a_{j,K,\mathbb{M}}} \leq \frac{1}{a_{K,\mathbb{M}}^2}\sum_{i,j=1}^{d} |\alpha_i|\,|\alpha_j| \\
&= \frac{1}{a_{K,\mathbb{M}}^2}(\sum_{i=1}^{d}|\alpha_i|)^2 \leq \frac{d}{a_{K,\mathbb{M}}^2}\sum_{i=1}^{d}\alpha_i^2.
\end{aligned}$$

Then,

$$\|(F_K')^{-1}\mathbb{M}_K^{-1}(F_K')^{-T}\| \leq \frac{d}{a_{K,\mathbb{M}}^2}\max_{\boldsymbol{\alpha}\neq 0} \frac{\sum_{i=1}^{d}\alpha_i^2}{\sum_{i,j=1}^{d}\alpha_i\alpha_j\hat{\nabla}\hat{\phi}_i^T\hat{\nabla}\hat{\phi}_j}. \tag{21}$$

We now establish a lower bound on the smallest eigenvalue of the matrix $B = (\hat{\nabla}\hat{\phi}_i^T\hat{\nabla}\hat{\phi}_j)_{i,j=1}^d$. Since $\hat{K}$ is equilateral, it has the same altitude and the same dihedral angle. This gives

$$\hat{\nabla}\hat{\phi}_i^T\hat{\nabla}\hat{\phi}_j = \begin{cases} \frac{1}{\hat{a}^2}, & i = j \\ -\frac{\cos(\hat{\alpha})}{\hat{a}^2} = -\frac{1}{d\,\hat{a}^2}, & i \neq j \end{cases}$$

where $\hat{\alpha}$ is the dihedral angle between the two faces of $\hat{K}$ not containing the i^{th} and j^{th} vertices each. Thus, B is a Z-matrix. Moreover, from $\sum_{j=0}^{d}\hat{\nabla}\hat{\phi}_j = 0$,

$$\sum_{j=1}^{d} B_{i,j} = \hat{\nabla}\hat{\phi}_i^T\sum_{j=1}^{d}\hat{\nabla}\hat{\phi}_j = -\hat{\nabla}\hat{\phi}_i^T\hat{\nabla}\hat{\phi}_0 = \frac{\cos(\hat{\alpha})}{\hat{a}^2} = \frac{1}{d\,\hat{a}^2} > 0.$$

This implies that B is an M-matrix. We have

$$\lambda_{\min}(B) \geq \min_i \sum_{j=1}^{d} B_{i,j} \geq \frac{1}{d\ \hat{a}^2}$$

and

$$\sum_{i,j=1}^{d} \alpha_i \alpha_j \hat{\nabla}\hat{\phi}_i^T \hat{\nabla}\hat{\phi}_j \geq \frac{1}{d\ \hat{a}^2} \sum_{i=1}^{d} \alpha_i^2.$$

Thus, from (21) we get

$$\|(F_K')^{-1}\mathbb{M}_K^{-1}(F_K')^{-T}\| \leq \frac{d^2\ \hat{a}^2}{a_{K,\mathbb{M}}^2},$$

which gives the right inequality of (20). □

Lemma 4.1 indicates that

$$\|(F_K')^{-1}\mathbb{M}_K^{-1}(F_K')^{-T}\| \sim a_{K,\mathbb{M}}^{-2} \tag{22}$$

if $\hat{K}$ is chosen to further satisfy $|\hat{K}| = \mathcal{O}(1)$.

It is also interesting to obtain a geometric interpretation for $\|(F_K')^T\mathbb{M}_K F_K'\|$. In this case, we do not need to require that $\hat{K}$ be equilateral.

Lemma 4.2. *Let $\hat{K}$ and K be two arbitrary simplexes in $\mathbb{R}^d$, $F_K : \hat{K} \to K$ the affine mapping between them, and $\mathbb{M}_K$ be a constant symmetric and positive definite matrix. Then,*

$$\frac{h_{K,\mathbb{M}}^2}{\hat{h}^2} \leq \|(F_K')^T\mathbb{M}_K F_K'\| \leq \frac{h_{K,\mathbb{M}}^2}{\hat{\rho}^2}, \tag{23}$$

where $h_{K,\mathbb{M}}$ is the diameter of K in the metric specified by $\mathbb{M}_K$ and $\hat{h}$ and $\hat{\rho}$ are the diameter and the in-diameter (defined as the diameter of the largest inscribed ellipsoid) of $\hat{K}$, respectively.

Proof. Consider any two points $\boldsymbol{\xi}_1, \boldsymbol{\xi}_2 \in \hat{K}$ and the corresponding points $\boldsymbol{x}_1, \boldsymbol{x}_2 \in K$. Then,

$$(\boldsymbol{x}_2 - \boldsymbol{x}_1) = F_K'(\boldsymbol{\xi}_2 - \boldsymbol{\xi}_1).$$

This gives

$$\begin{aligned}(\boldsymbol{x}_2 - \boldsymbol{x}_1)^T\mathbb{M}_K(\boldsymbol{x}_2 - \boldsymbol{x}_1) &= (\boldsymbol{\xi}_2 - \boldsymbol{\xi}_1)^T(F_K')^T\mathbb{M}_K F_K'(\boldsymbol{\xi}_2 - \boldsymbol{\xi}_1) \\ &\leq \|(F_K')^T\mathbb{M}_K F_K'\| \cdot \|\boldsymbol{\xi}_2 - \boldsymbol{\xi}_1\|^2 \\ &\leq \hat{h}^2\|(F_K')^T\mathbb{M}_K F_K'\|.\end{aligned} \tag{24}$$

Since $\boldsymbol{x}_1, \boldsymbol{x}_2 \in K$ are arbitrary,

$$h_{K,\mathbb{M}}^2 \leq \hat{h}^2\ \|(F_K')^T\mathbb{M}_K F_K'\|,$$

which gives the left inequality of (23).

Now consider two arbitrary opposing points $\boldsymbol{\xi}_1$ and $\boldsymbol{\xi}_2$ on the sphere of the largest inscribed ball of $\hat{K}$ (with the diameter $\hat{\rho}$). Dividing both sides of (24) by $\|\boldsymbol{\xi}_1 - \boldsymbol{\xi}_2\|^2 = \hat{\rho}^2$, we get

$$\frac{(\boldsymbol{x}_2 - \boldsymbol{x}_1)^T \mathbb{M}_K (\boldsymbol{x}_2 - \boldsymbol{x}_1)}{\hat{\rho}^2} = \frac{(\boldsymbol{\xi}_2 - \boldsymbol{\xi}_1)^T (F_K')^T M_K F_K' (\boldsymbol{\xi}_2 - \boldsymbol{\xi}_1)}{\|\boldsymbol{\xi}_1 - \boldsymbol{\xi}_2\|^2}.$$

Taking the maximum over all points on the sphere of the largest inscribed ball, the right-hand side is equal to $\|(F_K')^T M_K F_K'\|$ while the left-hand side is less than $h_{K,M}^2/\hat{\rho}^2$. Hence,

$$\|(F_K')^T M_K F_K'\| \le \frac{h_{K,M}^2}{\hat{\rho}^2},$$

which gives the right inequality of (23). □

Lemma 4.2 implies that $\|(F_K')^T \mathbb{M}_K F_K'\|$ is equivalent to $h_{K,\mathbb{M}}^2$, i.e.,

$$\|(F_K')^T \mathbb{M}_K F_K'\| \sim h_{K,\mathbb{M}}^2, \tag{25}$$

when $\hat{K}$ is chosen to be a unitary equilateral simplex.

Note that interchanging the roles of K and $\hat{K}$ and replacing $\mathbb{M}_K$ by $\mathbb{M}_K^{-1}$ in Lemma 4.2 provide bounds for $\|(F_K')^{-1} \mathbb{M}_K^{-1} (F_K')^{-T}\|$ as well. However, these bounds are not as sharp as bounds in Lemma 4.1.

4.2 Mesh nonsingularity

We first consider the semi-discrete MMPDE (16). In practical computation, proper modifications of the MMPDE for boundary vertices are required. Since the analysis is similar for the MMPDE with or without these modifications, for simplicity in the following we consider only the case without modifications.

Theorem 4.1. *Assume that the meshing functional (2) satisfies the coercivity condition*

$$G(\mathbb{J}, \det(\mathbb{J}), \mathbb{M}, \boldsymbol{x}) \ge \alpha \left[\mathrm{tr}(\mathbb{J}\mathbb{M}^{-1}\mathbb{J}^T)\right]^q - \beta, \quad \forall \boldsymbol{x} \in \Omega, \tag{26}$$

with $q > d/2$, where $\alpha > 0$ and $\beta \ge 0$ are constants. Assume also that the computational mesh $\mathcal{T}_c$ is chosen so that each of its elements is almost congruent to $N^{-\frac{1}{d}}\hat{K}$ up to rotation and translation, where $\hat{K}$ is the reference element taken to be a unitary equilateral simplex. If the elements of the mesh trajectory of the semi-discrete MMPDE (16) have positive volumes initially, they will have positive volumes for $t > 0$. Moreover, their minimum altitudes in the metric $\mathbb{M}$ and their volumes are bounded below by

$$a_{K,\mathbb{M}} \ge C\overline{m}^{-\frac{d}{2(2q-d)}} N^{-\frac{2q}{d(2q-d)}}, \quad \forall K \in \mathcal{T}_h, \quad \forall t > 0, \tag{27}$$

$$|K| \ge C\overline{m}^{-\frac{d^2}{2(2q-d)} - \frac{d}{2}} N^{-\frac{2q}{(2q-d)}}, \quad \forall K \in \mathcal{T}_h, \quad \forall t > 0, \tag{28}$$

where C is a positive constant depending only on the initial mesh.

Proof. Recall that (16) is a gradient system. As a consequence,

$$\frac{dI_h}{dt} = \sum_{i=1}^{N_v} \frac{\partial I_h}{\partial \boldsymbol{x}_i} \frac{d\boldsymbol{x}_i}{dt} = -\sum_{i=1}^{N_v} \frac{P_i}{\tau} \left\| \frac{\partial I_h}{\partial \boldsymbol{x}_i} \right\|^2 \leq 0. \tag{29}$$

This implies

$$I_h(\mathcal{T}_h(t)) \leq I_h(\mathcal{T}_h(0)), \tag{30}$$

where $\mathcal{T}_h(t) \equiv (\boldsymbol{x}_1(t), \cdots, \boldsymbol{x}_{N_v}(t))$ is the mesh at time t. From the coercivity (26), we get

$$I_h(\mathcal{T}_h(t)) \geq \alpha \sum_{K \in \mathcal{T}_h} |K| \left[\mathrm{tr}((\hat{E}_K E_K^{-1}) \mathbb{M}_K^{-1} (\hat{E}_K E_K^{-1})^T) \right]^q - \beta |\Omega|. \tag{31}$$

Since, by assumption, K_c is almost congruent to $N^{-\frac{1}{d}} \hat{K}$ (up to rotation and translation),

$$\hat{E}_K \approx N^{-\frac{1}{d}} \mathcal{Q}_K \hat{E},$$

where $\mathcal{Q}_K$ is a rotation operator and $\hat{E}$ is the edge matrix for $\hat{K}$. Inserting this into (31) gives

$$I_h(\mathcal{T}_h(t)) \geq C N^{-\frac{2q}{d}} \sum_{K \in \mathcal{T}_h} |K| \left(\mathrm{tr}(\hat{E} E_K^{-1} \mathbb{M}_K^{-1} E_K^{-T} \hat{E}^T) \right)^q - \beta |\Omega|.$$

From Lemma 4.1 (with $(F_K')^{-1} = \hat{E} E_K^{-1}$) and (30), we have

$$\sum_{K \in \mathcal{T}_h} |K| \cdot \frac{1}{a_{K,\mathbb{M}}^{2q}} \leq C N^{\frac{2q}{d}}, \tag{32}$$

where C depends on the initial mesh through the initial discrete functional $I_h(\mathcal{T}_h(0))$. Moreover, from (1) we have

$$|K| = \frac{|K| \sqrt{\det(\mathbb{M}_K)}}{\sqrt{\det(\mathbb{M}_K)}} \geq C_1 \frac{a_{K,\mathbb{M}}^d}{\overline{m}^{\frac{d}{2}}},$$

for some positive constant C_1 depending on d. Combining this with (32) leads to

$$\sum_{K \in \mathcal{T}_h} \frac{1}{a_{K,\mathbb{M}}^{2q-d}} \leq C \overline{m}^{\frac{d}{2}} N^{\frac{2q}{d}}, \tag{33}$$

which gives rise to (27) and (28).

Finally, the volumes of the elements will stay positive: from (17)-(19) we see that the nodal mesh velocities are bounded when $|K|$ is bounded from below as in (28). As a consequence, the mesh vertices will move continuously with time and the volumes of the elements cannot jump over the bound (28) to become negative. Thus, the volumes of the elements will stay positive (and bounded from below) if they are positive initially. □

Remark 4.1. From inequality (27) we can see that the ratio of $a_{K,\mathbb{M}}$ to the average element diameter, $N^{-\frac{1}{d}}$, is bounded below by

$$\frac{a_{K,\mathbb{M}}}{N^{-\frac{1}{d}}} \geq C \overline{m}^{-\frac{d}{2(2q-d)}} N^{-\frac{1}{(2q-d)}}, \quad \forall K \in \mathcal{T}_h. \tag{34}$$

This implies that the larger q is, the closer $a_{K,\mathbb{M}}$ is to the average element diameter. In particular, when $q \to \infty$, we have $a_{K,\mathbb{M}} \to \mathcal{O}(N^{-\frac{1}{d}})$ and the mesh is close to being quasi-uniform. Similarly, from (28) we have

$$\frac{|K|}{N^{-1}} \geq C\overline{m}^{-\frac{d^2}{2(2q-d)}-\frac{d}{2}} N^{-\frac{d}{(2q-d)}}, \quad \forall K \in \mathcal{T}_h. \tag{35}$$

For example, for Huang's functional (11) in 2D with $p = 1.5$ and $q = pd/2 = 1.5$ we have $|K| \gtrsim N^{-3}$. Note that this is a rather pessimistic worst case estimate. Recall that the functional (11) is designed to make the mesh to satisfy the equidistribution and alignment conditions as closely as possible. The equidistribution condition takes the form

$$|K|\sqrt{\det(\mathbb{M}_K)} = \frac{\sigma_h}{N}, \quad K \in \mathcal{T}_h$$

where $\sigma_h = \sum_K |K|\sqrt{\det(\mathbb{M}_K)}$. Thus, when a mesh closely satisfies this condition we have

$$\frac{|\Omega|}{N}\left(\frac{\underline{m}}{\overline{m}}\right)^{\frac{d}{2}} \leq |K| \leq \frac{|\Omega|}{N}\left(\frac{\overline{m}}{\underline{m}}\right)^{\frac{d}{2}}, \quad K \in \mathcal{T}_h$$

which implies $|K| = \mathcal{O}(N^{-1})$. This has been observed in numerical experiment; e.g., see Example 5.2 and Fig. 2f in Sect. 5. □

Remark 4.2. The key point of the proof is the energy decreasing property (29). This property is a crucial advantage of the geometric discretization (15) over discretizations based on the continuous MMPDE (6) which, generally speaking, cannot be guaranteed to be a gradient system. Another key component of the proof is the coercivity assumption (26). Once again, this may not be preserved in general by discretizations based on the continuous MMPDE (6). □

Remark 4.3. It can be seen that Huang's functional (11) satisfies the coercivity assumption (26) with $p > 1$ whereas Winslow's functional does not. In the latter case, we have $q = 1$ and (32) still holds. But (32) with $q = 1$ is not sufficient to guarantee a lower bound for $a_{K,\mathbb{M}}$.

It is worth pointing out that the functional of Huang and Russell [18, Example 6.2.3] also satisfies the coercivity assumption (26) for $p > 1$. □

Remark 4.4. The quantity I_h defined in (15) can be viewed as a measure for mesh quality. The smaller I_h is, the better the mesh quality. Then, (29) implies that the mesh quality improves when t increases. □

We now consider the time integration of (16). Denote the time instants by $t_n,\ n = 0, 1, \ldots$ with the property $t_n \to \infty$ as $n \to \infty$. We are interested in one-step methods in the form

$$\mathcal{T}_h^{n+1} = \Phi^n(\mathcal{T}_h^n), \quad n = 0, 1, \ldots, \tag{36}$$

for integrating MMPDE (16). From the proof of Theorem 4.1, we have seen that it is important that the discrete functional I_h is monotonically decreasing with the mesh trajectory. Thus, we assume that the scheme has the property

$$I_h(\mathcal{T}_h^{n+1}) \leq I_h(\mathcal{T}_h^n), \quad n = 0, 1, \ldots, \tag{37}$$

Many schemes, such as Euler's, the backward Euler, and algebraically stable Runge-Kutta schemes (including Gauss and Radau IIA schemes) can be used for this purpose under a time-step restriction involving a local Lipschitz bound of the Hessian matrix of I_h (e.g., [8, 29]).

Theorem 4.2. *Assume that the assumptions of Theorem 4.1 are satisfied, a numerical scheme in the form (36) is applied to MMPDE (16) and the resulting mesh sequence $\{\mathcal{T}_h^n\}_{n=0}^{\infty}$ satisfies the property of monotonically decreasing energy (37).*

If the time step is sufficiently small (but not diminishing) and the elements of the mesh trajectory have positive volumes initially, they will have positive volumes for all $t_n > 0$. Moreover, the minimum altitudes in the metric $\mathbb{M}$ and the element volumes are bounded from below by (27) and (28).

Proof. The proof of (27) and (28) for the fully discrete case is similar to that of Theorem 4.1 for the semi-discrete case. We only need to show that the volumes of the elements will stay positive if the time step is sufficiently small. To this end, we recall that G is assumed to be sufficiently smooth and $\mathbb{M}$ is bounded below and above (cf. (1)). A close examination on (17)-(19) shows that the mesh velocities have a upper bound independent of the elements and time instants when the mesh satisfies (27) and (28). Since the minimal altitude and, hence, the minimal distance between vertices have a lower positive bound (c.f. (27)), the elements will not become inverted and their volumes will stay positive if the time step is chosen small enough (smaller than the ratio of the minimal altitude to the maximal nodal velocity). (Note that this ratio is also independent of the elements and time instants and thus the time step is not diminishing.) The argument can be repeated for the next time step since the new mesh satisfies (27) and (28), too. Thus, the volumes of the elements stay positive for $t_n > 0$. □

4.3 Existence of limiting meshes and minimizers

We now investigate the convergence of the mesh trajectory as $t \to \infty$. First, we consider the semi-discrete case (16) and then the fully discrete case.

Theorem 4.3. *Under the assumptions of Theorem 4.1, for any nonsingular initial mesh, the mesh trajectory $\{\mathcal{T}_h(t), t > 0\}$ of MMPDE (16) has the following properties.*

(a) $I_h(\mathcal{T}_h(t))$ has a limit as $t \to \infty$, i.e.,

$$\lim_{t\to\infty} I_h(\mathcal{T}_h(t)) = L. \tag{38}$$

(b) The mesh trajectory has limiting meshes, all of which are nonsingular and satisfy (27) and (28).

(c) The limiting meshes are critical points of I_h, i.e., they satisfy

$$\frac{\partial I_h}{\partial \boldsymbol{x}_i} = 0, \quad i = 1, \ldots, N_v. \tag{39}$$

Proof. (a) $I_h(\mathcal{T}_h(t))$ has a limit since it is monotone, decreasing as $t \to \infty$ and bounded from below by $-\beta|\Omega|$.

(b) Theorem 4.1 implies that the mesh stays nonsingular for $t > 0$ and its vertices remain on $\overline{\Omega}$ (the closure of Ω). The compactness of $\overline{\Omega}$ means that $\{\mathcal{T}_h(t), t > 0\}$ has limits as $t \to \infty$. Obviously, the limiting meshes satisfy (27) and (28) and thus are nonsingular.

(c) Consider a convergent mesh sequence $\mathcal{T}_h(t_k)$, $k = 1, 2, ...$, with the limit $\mathcal{T}_h^*$. We will prove that $\mathcal{T}_h^*$ satisfies (39) using the contradiction argument: assume that $\mathcal{T}_h^*$ does not satisfy (39). Take a small positive number $\epsilon > 0$ and choose a mesh sequence $\tilde{\mathcal{T}}_h(t_k) \equiv \mathcal{T}_h(t_k + \epsilon)$, $k = 1, 2, \ldots$. From the compactness of $\overline{\Omega}$, we can choose a convergent subsequence from $\{\tilde{\mathcal{T}}_h(t_k)\}$. Without loss of generality, we pass the notation and consider $\{\tilde{\mathcal{T}}_h(t_k)\}$ as the subsequence with the limit $\mathcal{T}_h^{**}$. From the definition of $\tilde{\mathcal{T}}_h(t_k)$ and Taylor's expansion, we have

$$\begin{aligned}
I_h(\mathcal{T}_h^{**}) &= \lim_{k\to\infty} I_h(\tilde{\mathcal{T}}_h(t_k)) \\
&= \lim_{k\to\infty} I_h(\ldots, \boldsymbol{x}_i(t_k) + \epsilon \frac{d\boldsymbol{x}_i}{dt}(t_k) + \mathcal{O}(\epsilon^2), \ldots) \\
&= \lim_{k\to\infty} \left(I_h(\mathcal{T}_h(t_k)) + \epsilon \sum_{i=1}^{N_v} \frac{\partial I_h}{\partial \boldsymbol{x}_i}(\mathcal{T}_h(t_k)) \frac{d\boldsymbol{x}_i}{dt}(t_k) + \mathcal{O}(\epsilon^2) \right) \\
&= \lim_{k\to\infty} \left(I_h(\mathcal{T}_h(t_k)) - \epsilon \sum_{i=1}^{N_v} \frac{P_i}{\tau} \left\| \frac{\partial I_h}{\partial \boldsymbol{x}_i}(\mathcal{T}_h(t_k)) \right\|^2 + \mathcal{O}(\epsilon^2) \right).
\end{aligned}$$

Since I_h and its first and second derivatives are bounded under the conditions (27) and (28), we can choose ϵ small enough such that the second term in the about equation dominates the higher order terms. Moreover, the second term is positive since we have assumed that $\mathcal{T}_h^*$ does not satisfy (39). Thus, from the above equation we get

$$I_h(\mathcal{T}_h^{**}) < I_h(\mathcal{T}_h^*).$$

But this contradicts with (38) since it implies that $I_h(\tilde{\mathcal{T}}_h(t_k)) - I_h(\mathcal{T}_h(t_k)) \to 0$ as $k \to \infty$ or $I_h(\mathcal{T}_h^{**}) - I_h(\mathcal{T}_h^*) = 0$. □

Theorem 4.4. *Under the assumptions of Theorem 4.2, for any nonsingular initial mesh, the mesh trajectory $\{\mathcal{T}_h^n, n = 0, 1, ...\}$ of the scheme (36) applied to MMPDE (16) has the following properties.*

(a) $I_h(\mathcal{T}_h^n)$ has a limit as $n \to \infty$, i.e.,

$$\lim_{n\to\infty} I_h(\mathcal{T}_h^n) = L. \tag{40}$$

(b) The mesh trajectory has limiting meshes. All of the those limiting meshes are nonsingular and satisfy (27) and (28).

(c) If we further assume that the scheme satisfies a stronger property of monotonically decreasing energy,

$$\begin{cases} I_h(\mathcal{T}_h^{n+1}) \le I_h(\mathcal{T}_h^n), & n = 0, 1, \ldots, \\ I_h(\mathcal{T}_h^{n+1}) < I_h(\mathcal{T}_h^n), & \text{if } \mathcal{T}_h^n \text{ is not a critical point,} \end{cases} \tag{41}$$

then the limiting meshes are critical points of I_h, i.e., they satisfy (39).

Proof. The proof for (a) and (b) is similar to that of Theorem 4.4. The proof for (c) is also similar to that of Theorem 4.4 except that we choose $\tilde{\mathcal{T}_h}^{n_k} = \mathcal{T}_h^{n_k+1}$, where $\mathcal{T}_h^{n_k}$ is a subsequence converging to $\mathcal{T}_h^*$. Then (c) can be proved using (41) and the contradiction argument. □

Theorems 4.3 and 4.4 state that the values of the functional for the mesh trajectory are convergent as time increases, which can be used as a stopping criterion for the computation. In general, however, there is no guarantee that the mesh trajectory converges. To guarantee the convergence, a stronger descent in the functional value or a stronger requirement on the meshing functional is needed. For example, if the time marching scheme satisfies

$$I_h(\mathcal{T}_h^{n+1}) \leq I_h(\mathcal{T}_h^n) - \alpha \sum_{i=1}^{N_v} \left\| \frac{\partial I_h}{\partial \boldsymbol{x}_i}(\mathcal{T}_h^n) \right\|^2, \quad n = 0, 1, \ldots, \tag{42}$$

for a positive constant α, which is a stronger monotonically decreasing energy property than (41), then we have

$$\sum_{n=0}^{\infty} \sum_{i=1}^{N_v} \left\| \frac{\partial I_h}{\partial \boldsymbol{x}_i}(\mathcal{T}_h^n) \right\|^2 < \infty,$$

which in turn means that

$$\sum_{i=1}^{N_v} \left\| \frac{\partial I_h}{\partial \boldsymbol{x}_i}(\mathcal{T}_h^n) \right\| \to 0 \quad \text{as} \quad n \to \infty.$$

Then, we may expect the mesh trajectory $\{\mathcal{T}_h^n, n = 0, 1, \ldots\}$ to converge since typically $(\mathcal{T}_h^{n+1} - \mathcal{T}_h^n)$ is proportional to the gradient of I_h.

On the other hand, a stronger condition can be placed on the meshing functional. In particular, $\{\mathcal{T}_h^n, n = 0, 1, \ldots\}$ is convergent if I_h has a unique critical point. To explain this, we consider a special example: the functional (11) with $\theta = \frac{1}{2}$ or the functional (12). In this case, we have

$$I_h = \frac{1}{2} \sum_{K \in \mathcal{T}_h} |K| \sqrt{\det(\mathbb{M}_K)} \left(\mathrm{tr}(\hat{E}_K E_K^{-1} \mathbb{M}_K^{-1} E_K^{-T} \hat{E}_K^T) \right)^{\frac{dp}{2}}, \quad \frac{dp}{2} \geq 1. \tag{43}$$

We show that I_h is strongly convex about the variables $\boldsymbol{\xi}_1, \ldots, \boldsymbol{\xi}_{N_v}$, for which it is sufficient to show the term $\left(\mathrm{tr}(\hat{E}_K E_K^{-1} \mathbb{M}_K^{-1} E_K^{-T} \hat{E}_K^T) \right)^{\frac{dp}{2}}$ to be convex about $E \equiv [\boldsymbol{\xi}_0^K, \ldots, \boldsymbol{\xi}_d^K]$ for any element K. Moreover, since

$$\frac{d}{d\beta} \beta^{\frac{dp}{2}} = \frac{dp}{2} \beta^{\frac{dp}{2}-1} \geq 0, \quad \frac{d^2}{d\beta^2} \beta^{\frac{dp}{2}} = \frac{dp}{2} (\frac{dp}{2} - 1) \beta^{\frac{dp}{2}-2} \geq 0,$$

from [18, Lemma 6.2.1] it suffices to show that $\beta \equiv \mathrm{tr}(\hat{E}_K E_K^{-1} \mathbb{M}_K^{-1} E_K^{-T} \hat{E}_K^T)$ is a convex function about E.

Let

$$\boldsymbol{e} = \begin{bmatrix} 1 \\ \vdots \\ 1 \end{bmatrix} \in \mathbb{R}^d, \quad E_\eta = \left[\boldsymbol{\eta}_0^K, \ldots, \boldsymbol{\eta}_d^K \right] \in \mathbb{R}^{d \times (d+1)},$$

where E_η is an arbitrary matrix representing a perturbation of E. The quadratic form of the Hessian of β with respect to E can be expressed as

$$\operatorname{tr}\left(\frac{\partial \operatorname{tr}\left(\frac{\partial \beta}{\partial E} E_\eta\right)}{\partial E} E_\eta\right),$$

where we have used the notation of scalar-by-matrix differentiation (cf. (9) and (10) and [12]). We first compute $\frac{\partial \beta}{\partial E}$. By examining the relation between E and $\hat{E}_K$, we get

$$\frac{\partial \beta}{\partial [\boldsymbol{\xi}_1^K, \ldots, \boldsymbol{\xi}_d^K]} = \frac{\partial \beta}{\partial \hat{E}_K}, \quad \frac{\partial \beta}{\partial \boldsymbol{\xi}_0^K} = -\boldsymbol{e}^T \frac{\partial \beta}{\partial \hat{E}_K},$$

which can be combined into

$$\frac{\partial \beta}{\partial E} = \begin{bmatrix} -\boldsymbol{e}^T \\ I \end{bmatrix} \frac{\partial \beta}{\partial \hat{E}_K},$$

where I is the d-by-d identity matrix. To find $\frac{\partial \beta}{\partial \hat{E}_K}$, we look at $\hat{E}_K$ as a function of t. Then,

$$\frac{\partial \beta}{\partial t} = \operatorname{tr}\left(\frac{\partial (\hat{E}_K E_K^{-1} \mathbb{M}_K^{-1} E_K^{-T} \hat{E}_K^T)}{\partial t}\right) = \operatorname{tr}\left(2 E_K^{-1} \mathbb{M}_K^{-1} E_K^{-T} \hat{E}_K^T \frac{\partial \hat{E}_K}{\partial t}\right),$$

which gives

$$\frac{\partial \beta}{\partial \hat{E}_K} = 2 E_K^{-1} \mathbb{M}_K^{-1} E_K^{-T} \hat{E}_K^T.$$

Thus,

$$\operatorname{tr}\left(\frac{\partial \beta}{\partial E} E_\eta\right) = \operatorname{tr}\left(2 \begin{bmatrix} -\boldsymbol{e}^T \\ I \end{bmatrix} E_K^{-1} \mathbb{M}_K^{-1} E_K^{-T} \hat{E}_K^T E_\eta\right).$$

Repeating the process,

$$\begin{aligned} \operatorname{tr}\left(\frac{\partial \operatorname{tr}\left(\frac{\partial \beta}{\partial E} E_\eta\right)}{\partial E} E_\eta\right) &= 2 \operatorname{tr}\left(E_\eta \begin{bmatrix} -\boldsymbol{e}^T \\ I \end{bmatrix} E_K^{-1} \mathbb{M}_K^{-1} E_K^{-T} \begin{bmatrix} -\boldsymbol{e} & I \end{bmatrix} E_\eta^T\right) \\ &= 2 \left\| E_\eta \begin{bmatrix} -\boldsymbol{e}^T \\ I \end{bmatrix} E_K^{-1} \mathbb{M}_K^{-\frac{1}{2}} \right\|_F^2 \geq 0, \end{aligned}$$

where $\|\cdot\|_F$ is the Frobenius matrix norm. The equality in the above equation holds if and only if

$$\boldsymbol{\eta}_0^K = \cdots = \boldsymbol{\eta}_d^K. \tag{44}$$

Thus, the quadratic form of I_h about $\boldsymbol{\xi}_1, \ldots, \boldsymbol{\xi}_{N_v}$ is zero if and only if the above equality holds for all $K_c \in \mathcal{T}_c$. Since at least one of the boundary vertices is held fixed and its perturbation must be zero, (44) applies that $E_\eta = 0$ for the element containing the boundary vertex and then other elements, which means that I_h is strongly convex. As a consequence, I_h has a unique critical point (which is the minimizer) when Ω_c is convex.

Notice that the above uniqueness result is for I_h as a function of the computational coordinates. For the convergence of the mesh trajectory for (16) or its discretization, we need the uniqueness

result for I_h as a function of the physical coordinates. We use the argument of the functional equivalence described in Sect. 2. We first notice that the continuous functional in (12) is the same as the discrete functional I_h in (43) for the piecewise linear mapping $\{F_K : K_c \to K,\ K \in \mathcal{T}_h\}$ and the piecewise constant metric tensor $\{\mathbb{M}_K,\ K \in \mathcal{T}_h\}$. From the functional equivalence, we can conclude that I_h *has a unique minimizer either as a function of the coordinates of the physical vertices as long as* Ω_c *is convex.* Then, the mesh trajectory is convergent.

5 Numerical examples

To demonstrate the theoretical findings, in particular the decrease of the meshing functional and the lower positive bound of the element volumes, we present numerical results obtained for several examples for mesh adaptation as well as mesh smoothing in two and three dimensions. Huang's functional (11) with $p = \frac{3}{2}$ and $\theta = \frac{1}{3}$ is used in the computation. The MMPDE (17) is integrated using Matlab explicit ODE solver *ode45* for the mesh smoothing situation and implicit ODE solver *ode15s* for the mesh adaptation situation.

Example 5.1 (2D smoothing). We use the MMPDE-based smoothing to improve the mesh quality: we start with an initial mesh, perturb it (Fig. 1a) and use $\mathbb{M} = I$ to smooth the perturbed mesh. Figs. 1b and 1c show the resulting mesh at $t = 1.0$ and $t = 3.0$. The functional is monotonically decreasing. The minimal element volume is also decreasing but seems to converge to a positive number and stay bounded from zero. This is consistent with Theorem 4.2 which states that the element volumes of the mesh is bounded below by a positive number.

Example 5.2 (2D mesh adaptation for the sine wave). In this example, the metric tensor $\mathbb{M}$ is based on optimizing the piecewise linear interpolation error measured in the the L^2-norm [11, 19],

$$\mathbb{M} = \det\left(\alpha I + |H(u)|\right)^{-\frac{1}{6}} \left[\alpha I + |H(u)|\right], \tag{45}$$

where $H(u)$ is the recovered Hessian of u, $|H(u)|$ is the eigen-decomposition of $H(u)$ with the eigenvalues being replaced by their absolute values, and the regularization parameter $\alpha > 0$ is chosen such that

$$\int_\Omega \sqrt{\det(\mathbb{M})}\, d\boldsymbol{x} = 2 \int_\Omega \det\left(|H(u)|\right)^{\frac{1}{3}} d\boldsymbol{x}. \tag{46}$$

We choose $\Omega = (0,1) \times (0,1)$ and

$$u(x,y) = \tanh\left(-20\left[y - 0.5 - 0.25\sin\left(2\pi x\right)\right]\right).$$

Figs. 2a to 2c show the adaptive mesh at three time instants: $t = 0$, 1.0, and 3.0 for a 30×30 initial mesh. As expected, the functional energy is monotonically decreasing (Fig. 2d) and, for a fixed N, $|K|_{\min}$ stays bounded from below (Fig. 2e). Moreover, Fig. 2f shows the change of $|K|_{\min}$ for a sequence of finer grids with $N \to \infty$ and it seems that $|K|_{\min} \sim N^{-1}$, which is in consistent with (35), which reads as $|K| \geq C\overline{m}^{-3}N^{-3}$ for this example.

Example 5.3 (3D smoothing, cami1a). This example demonstrates smoothing of a tetrahedral mesh obtained by *TetGen* [28] for *cami1a* part (Fig. 3a). For this example too, the functional is monotonically decreasing and $|K|_{\min}$ stays bounded from below. Additionally, we compare

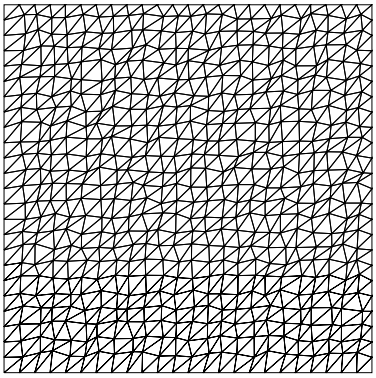

(a) perturbed initial mesh, $t = 0$

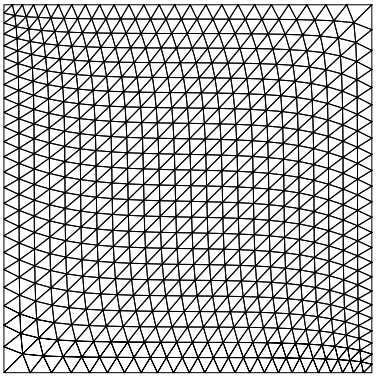

(b) smoothed mesh at $t = 1.0$

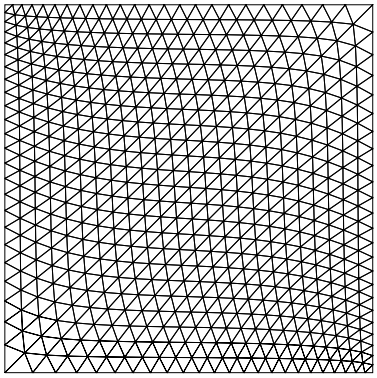

(c) smoothed mesh at $t = 3.0$

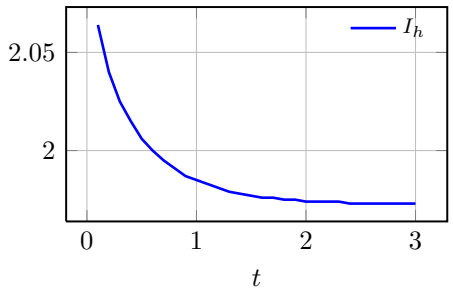

(d) I_h as function of t

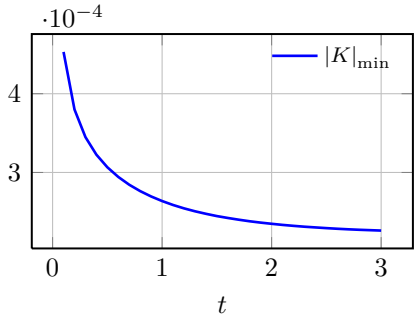

(e) $|K|_{\min}$ as function of t

Figure 1: Example 5.1 (2D smoothing)

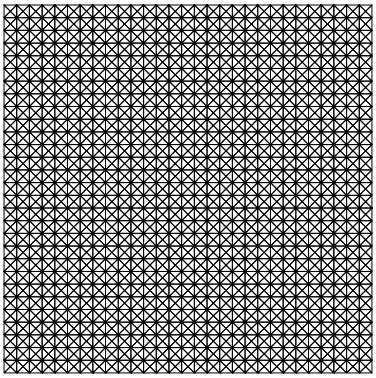

(a) initial mesh at $t = 0.0$

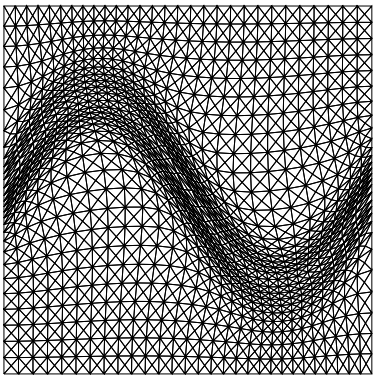

(b) adaptive mesh at $t = 1.0$

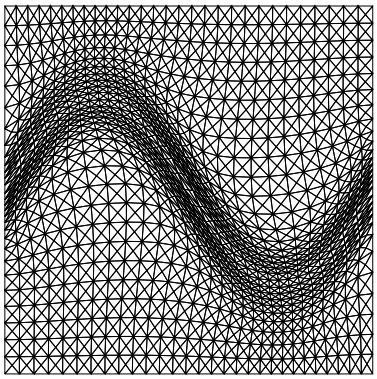

(c) adaptive mesh at $t = 3.0$

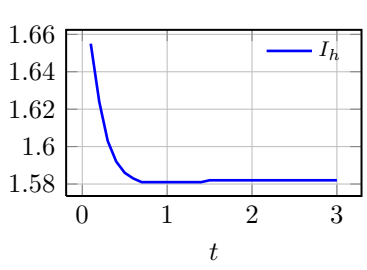

(d) I_h as function of t

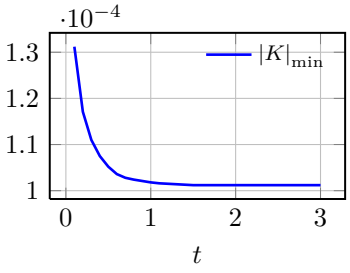

(e) $|K|_{min}$ as function of t

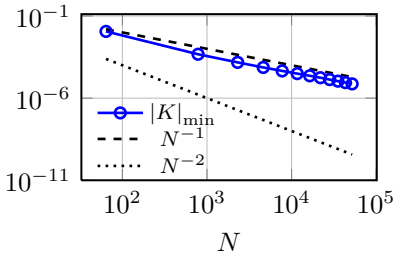

(f) $|K|_{min}$ and N^{-1} as $N \to \infty$

Figure 2: Example 5.2 (2D mesh adaptation for the sine wave)

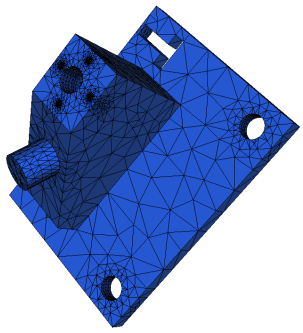

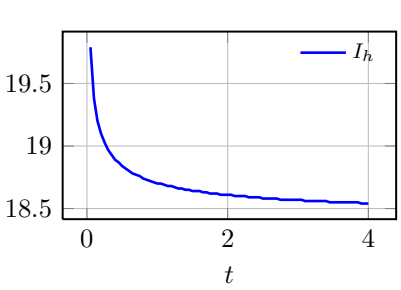

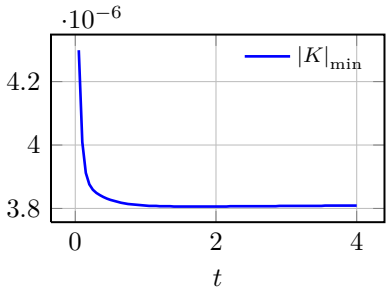

(a) mesh geometry (b) I_h as function of t (c) $|K|_{\min}$ as function of t

(d) statistics of dihedral angles before and after smoothing

angle	before	after	angle	before	after
0 – 5	2		80 – 110	25 178	25 025
5 – 10	280	8	110 – 120	4 858	5 186
10 – 20	3 372	2 280	120 – 130	3 896	4 761
20 – 30	6 673	7 036	130 – 140	2 557	3 315
30 – 40	11 001	12 385	140 – 150	1 448	1 256
40 – 50	13 227	13 911	150 – 160	793	163
50 – 60	14 754	14 697	160 – 170	284	5
60 – 70	12 158	12 308	170 – 175		
70 – 80	13 399	11 544	175 – 180		

Figure 3: Example 5.3 (3D smoothing, cami1a example, 18 980 elements)

the dihedral angle statistics of the original *TetGen* mesh with those after mesh smoothing. As it can be observed from Fig. 3d, smoothing significantly reduces the number of small (0°–20°) and large (150°–180°) dihedral angles and thus produce a more uniform mesh.

Example 5.4 (3D mesh adaptation for nine spheres). In this example we choose $\Omega = (-1,1)\times(-1,1)\times(-1,1)$ and $\mathbb{M}$ to minimize the L^2 interpolation error bound (see Example 5.2 on the choice of $\mathbb{M}$) for

$$\begin{aligned} u(x,y,z) = &\tanh\left(30\left[(x-0.0)^2+(y-0.0)^2+(z-0.0)^2-0.1875\right]\right)\\ &+\tanh\left(30\left[(x-0.5)^2+(y-0.5)^2+(z-0.5)^2-0.1875\right]\right)\\ &+\tanh\left(30\left[(x-0.5)^2+(y+0.5)^2+(z-0.5)^2-0.1875\right]\right)\\ &+\tanh\left(30\left[(x+0.5)^2+(y-0.5)^2+(z-0.5)^2-0.1875\right]\right)\\ &+\tanh\left(30\left[(x+0.5)^2+(y+0.5)^2+(z-0.5)^2-0.1875\right]\right)\\ &+\tanh\left(30\left[(x-0.5)^2+(y-0.5)^2+(z+0.5)^2-0.1875\right]\right)\\ &+\tanh\left(30\left[(x-0.5)^2+(y+0.5)^2+(z+0.5)^2-0.1875\right]\right)\\ &+\tanh\left(30\left[(x+0.5)^2+(y-0.5)^2+(z+0.5)^2-0.1875\right]\right) \end{aligned}$$

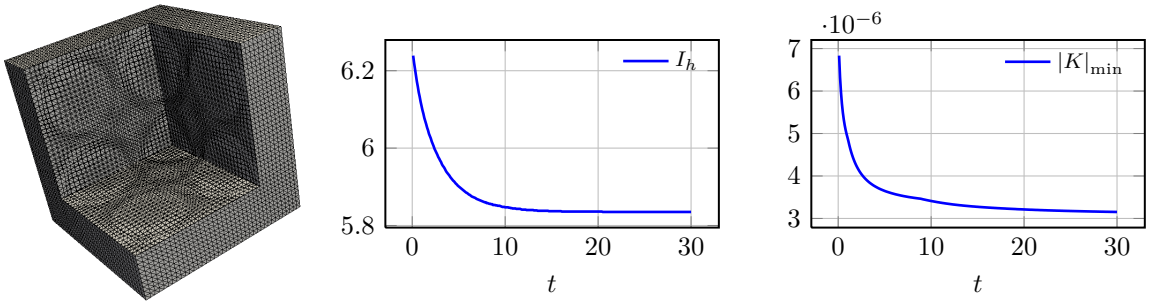

(a) mesh clip (b) I_h as function of t (c) $|K|_{\min}$ as function of t

Figure 4: Example 5.4 (3D mesh adaptation for nine spheres)

$$+ \tanh\left(30\left[(x+0.5)^2+(y+0.5)^2+(z+0.5)^2-0.1875\right]\right).$$

Fig. 4 shows an example of the final adaptive mesh and plots of the functional value and $|K|_{\min}$ with respect to the time. As expected, the functional value is monotonically decreasing. $|K|_{\min}$ is decreasing with time as well but one observes that it is bounded from below.

6 Conclusions

We have considered a geometric discretization recently introduced in [12] for meshing functionals and formulated the MMPDE as a modified gradient system of the corresponding discrete functionals for the location of mesh vertices. The main results are stated in Theorems 4.1–4.4.

Specifically, for meshing functionals satisfying the coercivity condition (26) with $q > d/2$ (such as Huang's functional (11) with $p > 1$), the mesh of the semi-discrete system (16) stays nonsingular for $t > 0$ if it is nonsingular initially. Moreover, the altitudes and the volumes of its elements are bounded below by positive numbers depending only on the number of elements, the metric tensor, and the initial mesh; cf. (27) and (28). Furthermore, the value of the meshing functional is always convergent as time increases, which can be used as a stopping criterion. Finally, the mesh trajectory has limiting meshes which satisfy (27) and (28), are nonsingular, and are critical points of the discrete functional. The convergence of the mesh trajectory can be guaranteed if a stronger condition is placed on the meshing functional.

It is shown in Theorems 4.2 and 4.4 that the above results also hold for fully discrete systems of (16) provided that the time step is sufficiently small and the underlying integration scheme for MMPDE (16) satisfies the property of monotonically decreasing energy (for example, Euler, backward Euler, algebraically stable Runge-Kutta schemes are known to preserve such a property with a mild restriction on the time step).

References

[1] G. Beckett, J. A. Mackenzie, and M. L. Robertson. A moving mesh finite element method for the solution of two-dimensional Stefan problems. *J. Comput. Phys.*, 168:500–518, 2001.

[2] J. U. Brackbill and J. S. Saltzman. Adaptive zoning for singular problems in two dimensions. *J. Comput. Phys.*, 46:342–368, 1982.

[3] G. F. Carey. *Computational grids: Generation, adaptation, and solution strategies.* Taylor & Francis, Washington, DC, 1997.

[4] A. S. Dvinsky. Adaptive grid generation from harmonic maps on Riemannian manifolds. *J. Comput. Phys.*, 95:450–476, 1991.

[5] L. A. Freitag and C. Ollivier-Gooch. Tetrahedral mesh improvement using swapping and smoothing. *Int. J. Numer. Meth. Engrg.*, 40(21):3979–4002, 1997.

[6] M. J. Gander and R. D. Haynes. Domain decomposition approaches for mesh generation via the equidistribution principle. *SIAM J. Numer. Anal.*, 50:2111–2135, 2012.

[7] I. M. Gelfand and S. V. Fomin. *Calculus of Variations.* Prentice-Hall, Inc., Englewood Cliffs, NJ, 1963.

[8] E. Hairer and C. Lubich. Energy-diminishing integration of gradient systems. *IMA J. Numer. Anal.*, 34:452–461, 2014.

[9] R. D. Haynes and F. Kwok. Discrete analysis of domain decomposition approaches for mesh generation via the equidistribution principal. *Math. Comp.*, 2015 (to appear).

[10] W. Huang. Variational mesh adaptation: isotropy and equidistribution. *J. Comput. Phys.*, 174:903–924, 2001.

[11] W. Huang. Metric tensors for anisotropic mesh generation. *J. Comput. Phys.*, 204:633–665, 2005.

[12] W. Huang and L. Kamenski. A geometric discretization and a simple implementation for variational mesh generation and adaptation. *J. Comp. Phys.*, 301:322–337, 2015.

[13] W. Huang, L. Kamenski, and H. Si. Mesh smoothing: an MMPDE approach. Research note at the 24th International Meshing Roundtable, WIAS Preprint No. 2130, 2015.

[14] W. Huang, Y. Ren, and R. D. Russell. Moving mesh methods based on moving mesh partial differential equations. *J. Comput. Phys.*, 113:279–290, 1994.

[15] W. Huang, Y. Ren, and R. D. Russell. Moving mesh partial differential equations (MMPDEs) based upon the equidistribution principle. *SIAM J. Numer. Anal.*, 31:709–730, 1994.

[16] W. Huang and R. D. Russell. A high dimensional moving mesh strategy. *Appl. Numer. Math.*, 26:63–76, 1998.

[17] W. Huang and R. D. Russell. Moving mesh strategy based upon a gradient flow equation for two dimensional problems. *SIAM J. Sci. Comput.*, 20:998–1015, 1999.

[18] W. Huang and R. D. Russell. *Adaptive Moving Mesh Methods*. Springer, New York, 2011. Applied Mathematical Sciences Series, Vol. 174.

[19] W. Huang and W. Sun. Variational mesh adaptation II: error estimates and monitor functions. *J. Comput. Phys.*, 184:619–648, 2003.

[20] P. Knupp and S. Steinberg. *Fundamentals of Grid Generation*. CRC Press, Boca Raton, 1994.

[21] P. M. Knupp. Jacobian-weighted elliptic grid generation. *SIAM J. Sci. Comput.*, 17:1475–1490, 1996.

[22] P. M. Knupp and N. Robidoux. A framework for variational grid generation: conditioning the Jacobian matrix with matrix norms. *SIAM J. Sci. Comput.*, 21:2029–2047, 2000.

[23] M. Křížek and Q. Lin. On diagonal dominance of stiffness matrices in 3D. *East-West J. Numer. Math.*, 3:59–69, 1995.

[24] R. Li, T. Tang, and P. W. Zhang. Moving mesh methods in multiple dimensions based on harmonic maps. *J. Comput. Phys.*, 170:562–588, 2001.

[25] V. D. Liseikin. *Grid Generation Methods*. Springer, Berlin, 1999.

[26] C. Lu, W. Huang, and J. Qiu. Maximum principle in linear finite element approximations of anisotropic diffusion-convection-reaction problems. *Numer. Math.*, 127:515–537, 2014.

[27] J. D. Pryce. On the convergence of iterated remeshing. *IMA J. Numer. Anal.*, 9:315–335, 1989.

[28] H. Si. TetGen, a Delaunay-based quality tetrahedral mesh generator. *ACM Trans. on Mathematical Software*, 41:Article No. 11, 2015. `http://www.tetgen.org`.

[29] A. M. Stuart and A. R. Humphries. *Dynamical Systems and Numerical Analysis*. Cambridge University Press, 1996.

[30] J. F. Thompson, Z. A. Warsi, and C. W. Mastin. *Numerical Grid Generation: Foundations and Applications*. North-Holland, New York, 1985.

[31] A. M. Winslow. Adaptive mesh zoning by the equipotential method. Technical Report UCID-19062, Lawrence Livemore Laboratory, 1981 (unpublished).

[32] X. Xu, W. Huang, R. D. Russell, and J. F. Williams. Convergence of de Boor's algorithm for generation of equidistributing meshes. *IMA J. Numer. Anal.*, 31:558–596, 2011.